

Article

Determining the Conditions That Lead to the Self-Extinguished and Self-Sustained Smoldering Combustion of Wood

Pengfei Ding ¹, Chunyin Zhang ², Qize He ^{1,*}, Lijing Wang ¹ and Yun Yang ^{1,*}

¹ Shanghai Fire Research Institute of MEM, Shanghai 200032, China; pf.ding@shfri.cn (P.D.); wanglijing@shfri.cn (L.W.)

² College of Safety Science and Engineering, Nanjing Tech University, Nanjing 210009, China; yzzhangcy1998@outlook.com

* Correspondence: heqize@shfri.cn (Q.H.); yangyun@shfri.cn (Y.Y.)

Abstract: To improve our understanding of flaming, smoldering, or self-extinction in the burning of wood, it is necessary to quantify the conditions that lead to self-extinguished and self-sustained smoldering combustion. Experiments were performed in a cone calorimeter under an external irradiation of 10 to 25 kW/m² to analyze the temperature and mass loss of self-extinguished and self-sustained smoldering. The smoldering front depth was the significant parameter used to capture the smoldering characteristic, and it was defined as the axial thickness that reaches the smoldering characteristic temperature. The critical smoldering front depth of self-extinguished smoldering was lower than 10–15 mm for 30 mm thick wood at 15.5 kW/m² irradiation. This critical depth decreased with the increase in heat flux, from 26.5 ± 1.5 mm at 10 kW/m² to 11 ± 1 mm at 25 kW/m². A simple theoretical analysis is proposed to explain the smoldering thickness threshold of self-sustained smoldering propagation based on the local heat balance. The equation predicts that the critical depth decreases as the heat flux increases, from 23.9 mm at 8 kW/m² to 7.3 mm at 25 kW/m². The predicted critical depth and heating duration were consistent with the experimental results. This study proposes a feasible parameter to help understand the threshold of smoldering propagation and the development of biomass burners.



Citation: Ding, P.; Zhang, C.; He, Q.; Wang, L.; Yang, Y. Determining the Conditions That Lead to the Self-Extinguished and Self-Sustained Smoldering Combustion of Wood. *Fire* **2024**, *7*, 60. <https://doi.org/10.3390/fire7020060>

Academic Editors: Mingjun Xu, Ruiyu Chen and Man Pun Wan

Received: 8 January 2024

Revised: 9 February 2024

Accepted: 15 February 2024

Published: 19 February 2024



Copyright: © 2024 by the authors. Licensee MDPI, Basel, Switzerland. This article is an open access article distributed under the terms and conditions of the Creative Commons Attribution (CC BY) license (<https://creativecommons.org/licenses/by/4.0/>).

Keywords: timber; smoldering propagation; self-extinction; self-sustained; char oxidation

1. Introduction

Wood is the most common natural material in forests, occupying 31% of the world's land [1]. Wood is one of the most renewable and sustainable construction materials and is widely used in ancient and green high-rise buildings [2]. Productive wood is also regarded as an important fuel resource for its high availability and ability to store heat [3]. However, the flammability of wood [4] raises serious public concerns about the fire safety of timber structures and wildlands. Continuous flaming or smoldering combustion [5–8] can cause the burnout of plenty of wooden fuel in timber structures and wildland fires [9], resulting in various combustion emissions and efficiencies [10,11]. The propagation of wood fire is essential knowledge for the structural design and process control of biomass combustion.

Smoldering is the slow, low-temperature, and flameless burning of porous fuels and is the most persistent type of combustion [12,13]. The engineered smoldering of wood is used to create scenarios that are highly robust and far from extinction and to generate the maximum amount of excess energy for subsequent scenarios [14], though it is highly affected by the environment and fuel and easily extinguished. In the laboratory environment, the self-extinction of wood flaming has been observed [15]. Recent research states that self-extinction appears to be an intrinsic quality of timber since the flame heat flux is not sufficient to sustain its burning, and the critical heat flux and mass loss rate of the flaming extinction of wood have been proposed and verified in small- and large-scale

fire tests [15–17]. However, a large knowledge gap exists regarding the self-extinction of smoldering combustion in wooden materials.

Smoldering propagation is controlled by the competition between oxygen supply and heat loss [12,18,19], and the thermal imbalance between the required heat supply and heat loss [20–22] results in a smoldering or no-smoldering state. Here, the heat supply is associated with the generation of the combustion controlled by the oxygen supply and external radiation. The heat loss is mainly the heat conduction of pyrolyzed char. The oxygen has difficulty diffusing into low-porosity materials, resulting in greater difficulty in maintaining char oxidation, resulting in the extinction of smoldering [23]. Although it will smolder to burn out with the applied external heat flux, this is still regarded as self-extinguished smoldering. For high-porosity materials like foam [24], cotton [25], and pine needles [26], smoldering can propagate to extinction without external irradiation, regarding self-sustained smoldering.

The self-extinguished or self-sustained smoldering combustion of wood is complex, and its criteria include a broad range of parameters. Some critical parameters associated with smoldering extinction have been proposed, such as the critical wind speed [27,28] and temperature threshold [29]. Gratkowski et al. [30] further speculated that the ignition depth of smoldering ignition is the key to self-extinguished or self-sustained smoldering. Several studies have analyzed the evolution of smoldering propagation from the perspective of the local and global energy balance [23,31,32]. Based on the heat transfer on the smoldering front, Liñán et al. [33] and Dosanjh et al. [34] established dimensionless number and smoldering propagation velocity formulas to forecast smoldering extinction, respectively. Zaroni et al. [14,35,36] proposed the concept of net energy based on the global energy balance and reproduced the self-sustained one-dimensional bitumen smoldering propagation accurately. However, these experiments mainly focus on the influence of the external environment (especially wind speed) on smoldering propagation. To the best of the authors' knowledge, few studies have systematically addressed the critical conditions required for the self-extinction and self-sustained smoldering of wooden material, which is more related to the properties of the combustion; thus, there is a large knowledge gap.

The purpose of this experimental study is to explore the limiting conditions of self-sustained and self-extinguished smoldering. Well-controlled experiments with different heating durations and heat fluxes were conducted. The axial temperature and mass loss during the whole smoldering process were measured, and then the characteristics of self-sustained and self-extinguished smoldering were analyzed. The critical parameter was defined as well. Afterward, an analytical model based on the heat balance of the smoldering front was proposed to further explain and verify the critical parameter, as well as the effect of external radiation.

2. Experiment

2.1. Materials

The wood used in this experiment was German beech, which was cut perpendicular to the grain to obtain cylindrical samples of wood. Cylindrical samples with a diameter of 60 mm and thickness of 30 mm were tested, as shown in Figure 1a. Their initial mass was 58 ± 5 g at an ambient temperature of 15 °C and relative humidity of 30%, and their bulk density was calculated to be 730 ± 30 kg/m³, with a moisture content (dry-mass basis) of $10.6 \pm 0.2\%$.

2.2. Setup and Test Procedures

The schematic diagram of the experimental apparatus is illustrated in Figure 1b, and it mainly consists of a cone-shaped heater, a sample container, and a precision scale. The heater was placed 25 mm above the sample, which provided uniform irradiation up to 100 kW/m² on the wood top surface. In addition, 16 cm diameter and 8 mm thick shutters were fixed below the heater, enabling the manual or automatic blocking of the radiation

exposure. Before the test, the irradiation could be varied by adjusting the heating power and calibrating it with a radiometer.

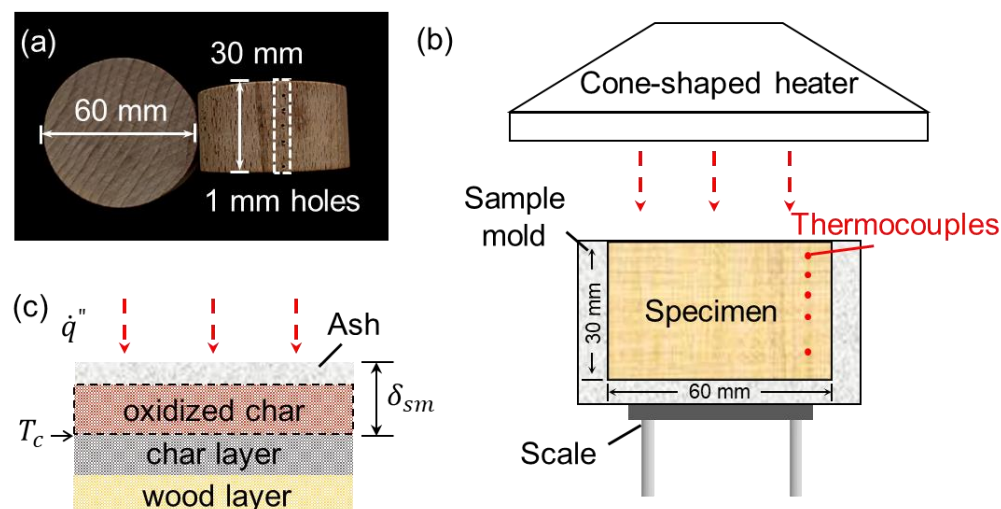


Figure 1. (a) Photos of the wood sample, (b) a schematic diagram of the experimental apparatus, and (c) schematics for smoldering characteristic temperature and smoldering depth.

During the experiment, the cylindrical specimen was tightly flush-mounted in an 80 mm squared fiberboard with a 60 mm diameter and 30 mm deep hollow cylinder in the center. The wall thickness of the mold was about 20 mm, which can effectively act as the insulation boundary, forming a one-dimensional smoldering propagation condition.

Throughout the experiment, the heat flux was fixed to 10, 15.5, and 25 kW/m², which will initiate smoldering propagation [6,8]. The mass evolution of the wood sample was measured by the electric balance (Mettler-Toledo XE10002S, resolution: 0.01 g). The surface and internal temperature of wood were carefully monitored using five 1 mm bead K-type thermocouple probes, which were inserted into the 10 mm depth pre-hole drilled by a 1 mm diameter drill bit at 5, 10, 15, 20, and 28 mm, as shown in Figure 1a. The small structural changes caused by perforation can be ignored since the experiment mainly focused on the heat transfer of wood smoldering. Because thermocouples might affect the mass measurement, the measurements of mass and temperature were conducted separately in repeating tests. To ensure repeatability, at least three experiments were conducted for each condition.

2.3. Smoldering Front Depth

The heterogeneous pathways of smoldering combustion can be broadly simplified as evaporation, devolatilization, and char oxidation. During the smoldering combustion, the raw sample was pyrolyzed to the char layer, and the internal heat released from the char oxidation may further pyrolyze the wood in depth, as illustrated in Figure 1c. The smoldering phenomenon has a low temperature of 350–700 °C, depending on the heat release and the oxygen that attacks the fuel surface [6,28,35,37]. Given a minimum smoldering (char oxidation) temperature (T_c), the average thickness of the smoldering front (δ_{sm}) at the moment when the external radiation is terminated can be estimated based on the thermocouple data. Figure 2 summarizes the thickness of the smoldering front at different moments when the irradiation is removed, and it increases with the heating duration. As the irradiation increases, the duration of the requested smoldering front depth decreases.

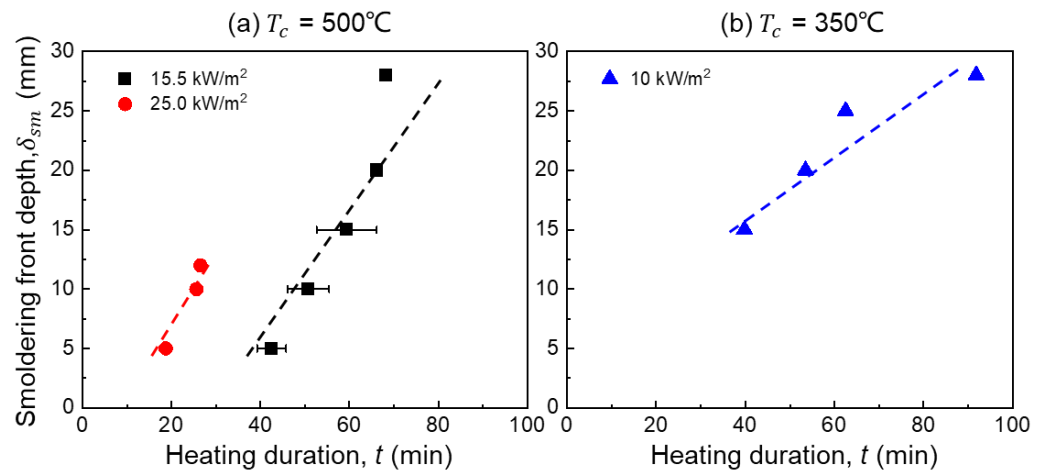


Figure 2. Smoldering front depth as a function of heating duration and heat flux for (a) $T_c = 500\text{ }^\circ\text{C}$ at 15 and 25 kW/m^2 and (b) $T_c = 350\text{ }^\circ\text{C}$ at 10 kW/m^2 .

The selection of characteristic temperatures under different heat fluxes relied on the pre-test that maintained the irradiation for the whole process of the smoldering propagation. For 15 and 25 kW/m^2 , all depths can reach and maintain $500\text{ }^\circ\text{C}$. For 10 kW/m^2 , temperatures below 25 mm depth can only reach about $350\text{ }^\circ\text{C}$, and this will be further explained in Section 3.3. The related smoldering front depth (δ_{sm}) and heating duration (t) for 10, 15.5, and 25 kW/m^2 are listed in Table 1. It is worth noting that the maximum smoldering front depth is equal to the thickness of the specimen, which is 30 mm in these experiments. This depth also means that the external heat flux existed throughout the smoldering process.

Table 1. The smoldering front depth and related heating duration in the experiment.

$\dot{q}'' = 25\text{ kW/m}^2$		$\dot{q}'' = 15.5\text{ kW/m}^2$		$\dot{q}'' = 10\text{ kW/m}^2$	
δ_d (mm)	t (min)	δ_d (mm)	t (min)	δ_d (mm)	t (min)
5	18.7	5	42.4 ± 3.2	–	–
10	25.6	10	50.8 ± 4.7	–	–
12	26.5	–	–	–	–
–	–	15	59.4 ± 6.4	15	39.8
–	–	20	66.1	20	53.2
–	–	–	–	25	62.5
–	–	28	68.2	28	91.8

3. Experimental Results

Depending on the external irradiation and its interaction with the fuel bed, no ignition, unsustainable (self-extinguished) smoldering, and self-sustained smoldering were observed. Unlike what occurs in other porous charring materials, smoldering propagation can be sustained once ignited [26]. An example of the repetition of the experiment is illustrated in Appendix A. For most conditions, the experiments reproduced the conclusions well. However, with the loose measurement methods, some of the data are incomplete. Therefore, we chose relatively complete experiments to express the pattern for self-extinguished and self-sustained smoldering.

3.1. Self-Extinguished and Self-Sustained Smoldering Phenomena

Figure 3a shows a group of thermocouple measurements of smoldering with a 5 mm smoldering front depth for the sample thickness of 30 mm under the irradiation of 15.5 kW/m^2 . It is noticed that although temperatures at multiple depths were measured, temperatures at the top (5 mm), bottom (28 mm), and given smoldering front depths were selected to characterize self-sustained or self-extinguished smoldering. The scattered points

represent the moment that the radiant heat flux was turned off, and the smoldering process can be divided into two phases: with (blue region) and without external radiation (yellow region). After a short period of heating, T_{-5} , showing a temperature of 5 mm below the surface, rapidly increased and reached the smoldering characteristic temperature (500 °C). Once the cone-shape heater was off, T_{-15} and T_{-28} first increased slightly but soon dropped below 300 °C, indicating that the smoldering fire became self-extinguished. At last, T_{-5} dropped below 200 °C, even lower than T_{-15} and T_{-28} . This is probably caused by the environmental convective cooling on the top surface. During this experimental process, strong smoke or volume change was observed, which is different from a smoldering peat fire, with difficulty in the detection of an underground smoldering fire in peatland [37,38].

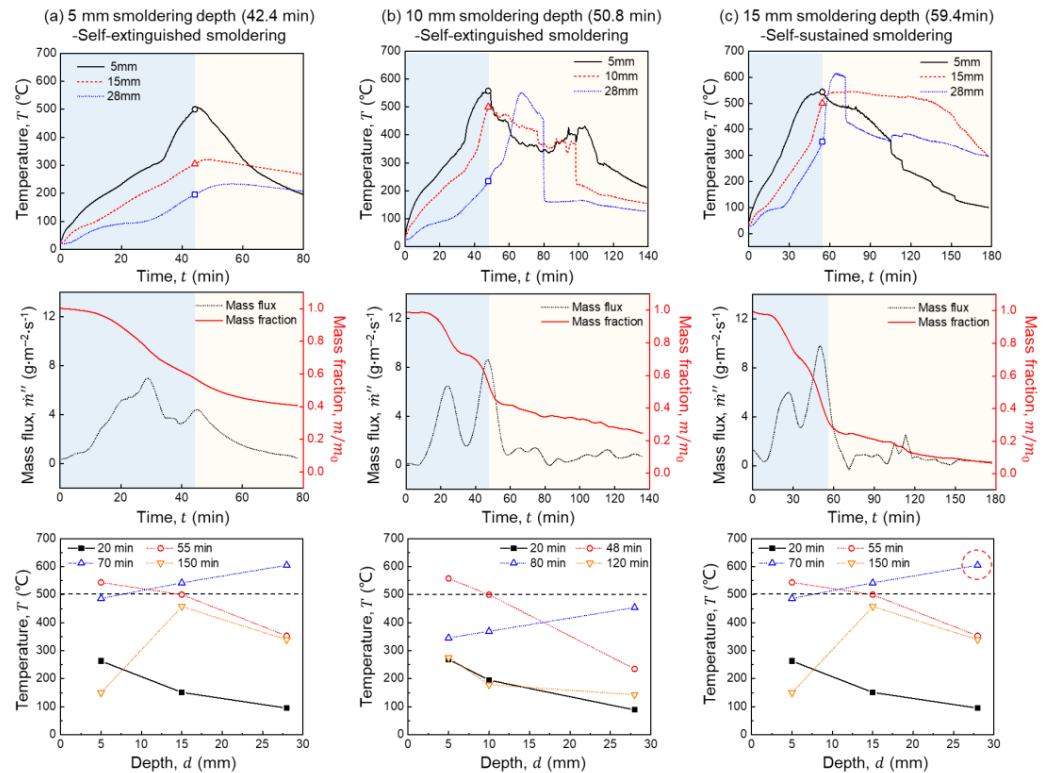


Figure 3. Thermocouple and mass measurement and temperature gradient of the smoldering propagation at (a) 5 mm, (b) 10 mm, and (c) 15 mm smoldering depth under the irradiation of 15.5 kW/m².

Figure 3a also presents the mass loss rate and mass fraction evolution of 5 mm smoldering depth. When the cone-shaped heater closed, mass was lost by about 40%, and the final mass loss was about 60%. The mass loss rate gradually decreased to 1 g/(m²·s) until smoldering was extinguished. Briefly, self-extinguished smoldering was a slow process lasting about 32 min for this smoldering front depth.

When the smoldering front depth was increased to 10 mm, as shown in Figure 3b, the specimen could only form self-sustained smoldering for a while and was eventually extinguished. The increase in T_{-5} at 80 min may be because of the touch of the glowing surface, which has a higher temperature. Despite some fluctuation, the thermocouple measurements are similar to the former measurement. Though the T_{-20} rise exceeded 500 °C, 20 min after the heater turned off, it could not maintain this level, and it dropped rapidly in a few minutes. The two peaks in mass loss rate at 20 and 50 min correspond to the flat of mass loss, which means that pyrolysis and oxidation reactions are dominant, respectively. The final consumed mass increased to ~80%, and the mass loss rate dropped to ~1 g/(m²·s) gradually as well. Generally, if the final residue was more than 20% and the temperature was not maintained as T_c , the specimen could be considered self-extinguished.

With a further increase in the smoldering front depth to 15 mm, as shown in Figure 3c, self-extinguished smoldering transforms into self-sustained smoldering. Once T_{-15} reached 500 °C and the external heater was turned off, it gradually increased and was unchanged after rising to 520 °C. Meanwhile, T_{-28} exceeded 350 °C and rose rapidly, reaching a maximum of 623 °C and maintaining it for 10 min, and then was reduced to 400 °C until the end. Correspondingly, mass loss was about 99% at the end. Therefore, if the final residue was nearly zero and the temperatures could reach and maintain the smoldering characteristic temperature, self-sustained smoldering can be considered to have occurred.

Figure 3 (bottom line) also illustrates the temperature gradient of 5, 10, and 15 mm smoldering front depth at different times. The solid and dashed lines connect with and without external heat flux, respectively. The red line represents the moment when the cone-shaped heater was turned off. Only at 15 mm smoldering depth, the internal temperature (T_{-28}) exceeds and maintains the smoldering characteristic temperature (500 °C). We can infer that the critical smoldering front depth of self-extinguished and self-sustained smoldering is 10~15 mm for the sample thickness of 30 mm under the irradiation of 15.5 kW/m².

3.2. Effect of Smoldering Front Depth on Smoldering Characteristics

Self-extinguished smoldering gradually transformed into self-sustained smoldering as the smoldering front depth increased. Figure 4a summarizes the axial smoldering propagation speed of different smoldering front depths for the sample thickness of 30 mm under the irradiation of 15.5 kW/m². For all self-sustained smoldering front depths, the smoldering propagation speed increases as the depth increases. For example, for the 20 mm smoldering front depth, the smoldering propagation speed increases from 0.11 mm/min at 5 mm to 2.31 mm/min at 28 mm. Once the external irradiation is turned off, the smoldering propagation speed will decay. However, for the large self-sustained smoldering depth, the effect of external radiation is less apparent.

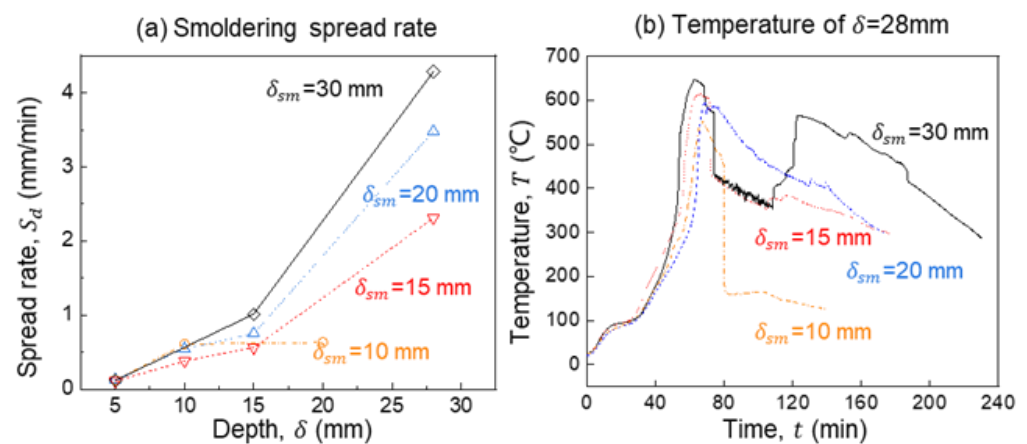


Figure 4. (a) Smoldering spread rate vs. depth and (b) thermocouple measurement of 28 mm depth at different smoldering depths for the sample thickness of 30 mm under the irradiation of 15.5 kW/m².

Similarly, this trend was clearer for temperatures of smoldering propagation. Figure 4b compares the thermocouple measurement of T_{-28} under different smoldering depths. For 10 mm smoldering depths (self-extinguished smoldering), T_{-28} would quickly drop below the pyrolysis temperature in a short time once the heater was turned off. However, for 15 and 20 mm smoldering depths, T_{-28} was consistent with that of the maximum smoldering depth (30 mm). The fluctuation at 100 min in Figure 4b is related to the deviation of the position of the thermocouples caused by the changes in structural characteristics and fuel composition during the smoldering combustion. It can be speculated that external radiation already does not affect smoldering propagation once the smoldering is self-sustained.

3.3. Effect of Heat Flux on the Critical Smoldering Front Depth

The critical smoldering front depth of self-extinguished and self-sustained smoldering will be significantly affected by external radiation. Figure 5 presents groups of thermocouples and mass measurements of wood smoldering with 10 and 12 mm smoldering front depths under the irradiation of 25 kW/m^2 . The scattered points and distinguishing regions are just like those in Section 3.2. radiation is less apparent.

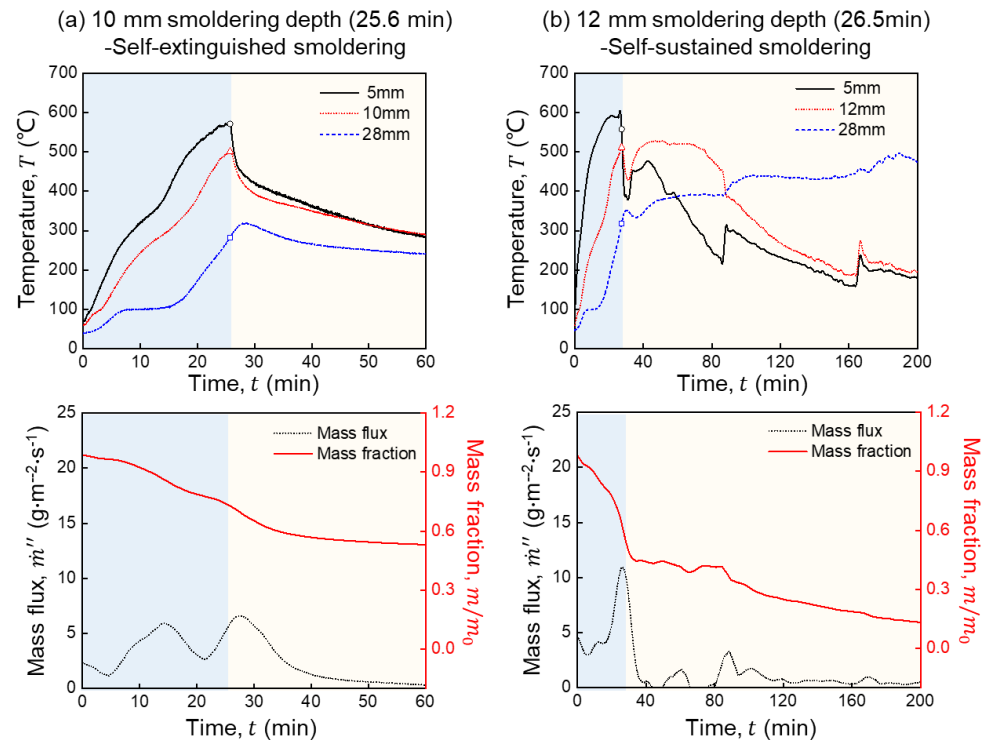


Figure 5. Temperature and mass measurements of the smoldering propagation at (a) 10 mm and (b) 12 mm smoldering depth under the irradiation of 25 kW/m^2 .

For the 10 mm smoldering front depth, as shown in Figure 5a, it was self-extinguished obviously. Once the cone-shaped heater was off, all the temperatures would quickly drop below $300 \text{ }^\circ\text{C}$, and the mass loss rate would also quickly drop to about $1 \text{ g/(m}^2\cdot\text{s)}$. The mass fraction reduced from 65% only to the final 55% as well. For the 10 mm smoldering front depth, as shown in Figure 5b, when the heater was turned off, T_{-5} and T_{-10} dropped rapidly at the beginning, and T_{-5} even dropped to $380 \text{ }^\circ\text{C}$. Interestingly, though T_{-28} increased continuously, it could not reach the smoldering characteristic temperature. This was probably because the oxygen had difficulty diffusing into this depth, limited by the char and ash layer on the sample surface [39]. The glowing combustion with higher temperatures could not be formed as well. However, it still indicated that the critical smoldering front depth of self-extinguished and self-sustained smoldering was 10–12 mm under 25 kW/m^2 .

As the heat flux decreased to 10 kW/m^2 , the critical depth increased significantly. Figure 6a,b show the thermocouple and mass measurement at 25 and 28 mm smoldering front depths, respectively. It seems that T_{-25} and T_{-28} cannot reach the former characteristic temperature of smoldering. This is because when the low irradiation and covering of the char layer are combined, T_c only relies on the heat released by the char oxidation, which does not have enough unburned fuel limited by the thickness. Therefore, we can roughly regard the smoldering characteristic temperature as $350 \text{ }^\circ\text{C}$, slightly lower than that at 15.5 and 25 kW/m^2 . For the 25 mm smoldering front depth, all temperatures dropped below $300 \text{ }^\circ\text{C}$ dramatically once the heater turned off, showing self-extinguished characteristics. It is worth noting that once the heater turned off, mass loss increased from 80% to 100%. This means that even though the smoldering combustion was not self-sustained, smoldering

propagation was thorough for this smoldering front depth limited by the fuel thickness. T_{-28} at the 28 mm smoldering front depth could be maintained at a given T_c and had certain self-sustained characteristics. For 10 kW/m^2 , it can still be considered that the critical smoldering front depth is 25–28 mm. radiation is less apparent.

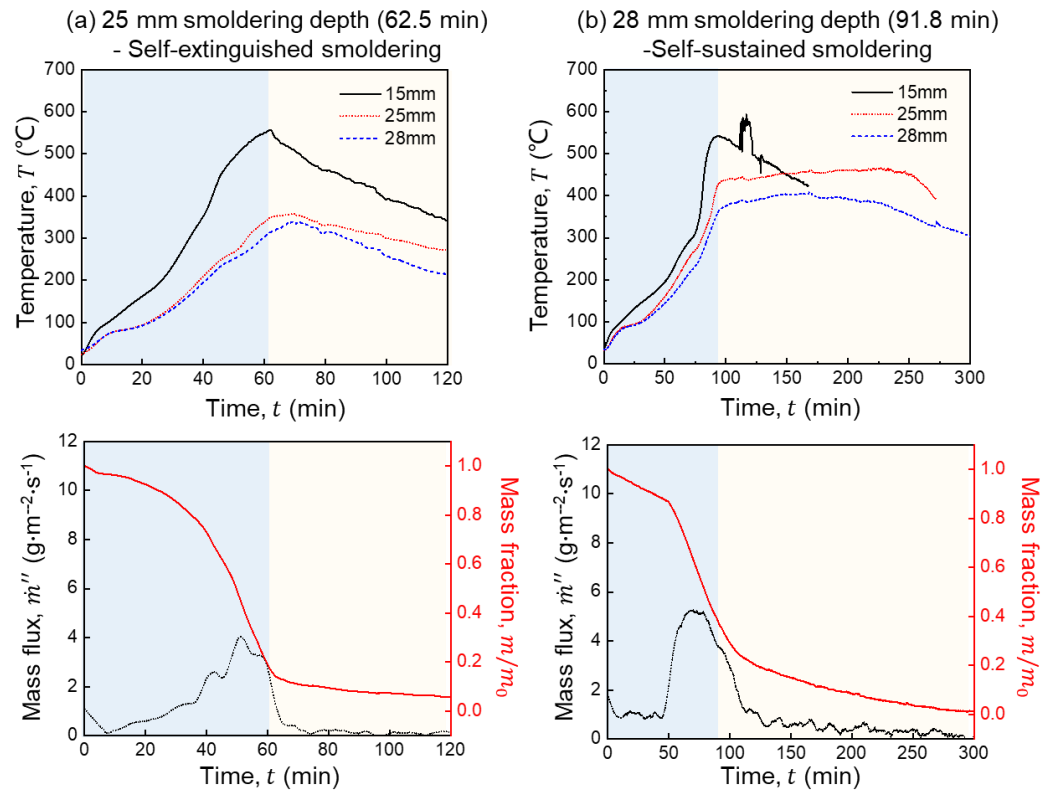


Figure 6. Temperature and mass measurements of the smoldering propagation at (a) 25 mm and (b) 28 mm smoldering depth under the irradiation of 10 kW/m^2 .

Figure 7 further summarizes the critical smoldering front depth of self-extinguished and self-sustained smoldering for the sample thickness of 30 mm under various external radiation levels. The error bars show the standard deviations of the values measured from the smoldering depth. radiation is less apparent.

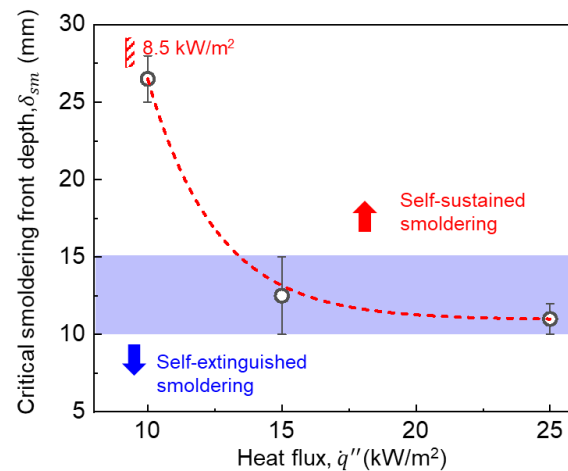


Figure 7. Critical smoldering depth of self-extinguished and self-sustained smoldering for different heat fluxes.

Beech could be ignited as smoldering at the range of $8.5\text{--}28 \text{ kW/m}^2$ [6]. The critical front depth decreases as heat flux increases, from $26.5 \pm 1.5 \text{ mm}$ at 10 kW/m^2 to $11 \pm 1 \text{ mm}$

at 25 kW/m². However, with an increase in the heat flux from 15 to 25 kW/m², the critical depth changes slightly. Once this depth is reached, self-sustained smoldering easily occurs, and the influence of external heat flux will become small. Overall, the ignited smoldering behavior of the specimen can be divided into the self-sustained and self-extinguished smoldering regions for different heat fluxes and smoldering front depths.

4. Discussion

Self-extinguished and self-sustained smoldering combustion has been observed, but it has not been studied in depth before. The critical smoldering front depth of the self-extinguished or self-sustained smoldering can be explained by the energy-conservation equation of the smoldering zone. In modeling, ideal one-dimensional smoldering propagation is assumed as pyrolysis and oxidation, so the fuel can be divided into smoldering, pyrolysis, and preheat zones as shown in Figure 8. It should be noted that the ash layer is not included in the smoldering zone, as the oxidation reaction has been completed. radiation is less apparent.

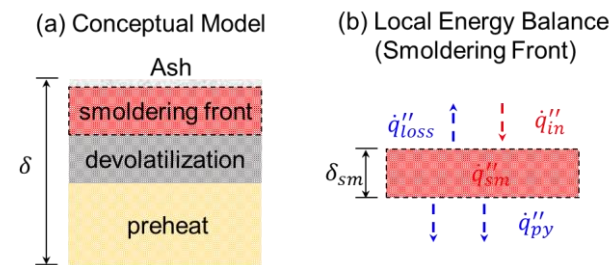


Figure 8. (a) Conceptual model and (b) local (smoldering front) energy balance of smoldering propagation.

To simplify the calculation, the decay of incident radiation caused by the top ash layer is ignored. The energy-conservation equation for 1D steady-state spread is

$$\rho c_p \frac{\partial T}{\partial t} = \frac{\partial}{\partial x} \left(\lambda \frac{\partial T}{\partial x} \right) + \dot{q}'''_{sm} \tag{1}$$

where the advective term neglects the small motion in the vertical direction due to a uniform vertical temperature profile after a uniform ignition; ρ and c_p are the sample density and heat capacity, respectively. On the right-hand side, \dot{q}'''_{sm} is the volumetric heat release from smoldering ($\dot{q}'''_{sm} = \rho\phi\Delta H_{ox}R_{ox}$) [36], λ is the thermal conductivity, T is the temperature of the solid phase, \dot{q}''_{loss} is the volumetric heat loss to the environment ($\dot{q}''_{loss} = h(T_c - T_o) + \epsilon\sigma(T_c^4 - T_0^4)$), \dot{q}''_{py} is the volumetric heat absorbed by pyrolysis ($\dot{q}''_{py} = \rho\phi(\delta - \delta_{sm})\Delta H_{py}R_{py}$) [15], and x is the vertical spread direction. And the boundary conditions of the top and bottom surfaces are

$$x = 0, -\lambda \frac{\partial T}{\partial x} = \dot{q}''_{in} - \dot{q}''_{loss} \tag{2}$$

$$x = \delta_{sm}, -\lambda \frac{\partial T}{\partial x} = \dot{q}''_{py} \tag{3}$$

respectively. Combining Equations (1)–(3), the smoldering front thickness is the minimum depth for self-sustained smoldering $\delta_{sm,min}$ [36] and can be further expressed as

$$\delta_{sm,min} = \frac{\dot{q}''_{py} + \dot{q}''_{loss} - \dot{q}''_{in}}{\dot{q}'''_{sm}} \tag{4}$$

It should be noted that R_{ox} and R_{py} are the reaction rates of char oxidation and pyrolysis, which are all set to be constant for simplification [8]. T_c and T_0 are the characteristic

temperature of smoldering and ambient temperature, obtained from our previous work [6]. Figure 9a illustrates the predicted and experimental results for the critical smoldering front depth at various heat fluxes. The experimental result at 6 kW/m² from Liang [40] is also considered. In particular, according to the experiment, T_c is set to 500 and 350 °C above and below 15 kW/m², respectively. The predicted critical depth decreases with the increasing heat flux, from 27.1 mm at 6 kW/m² to 7.3 mm at 25 kW/m², and is slightly lower than that in the experiment. This may be because of the presented external radiation. Based on the results, self-sustained and self-extinguished smoldering behavior regions can be further summarized. Although the relationship relies on certain parameters, it provides a decided relation between smoldering front depth and self-sustained smoldering propagation. More experiments will be conducted to verify it in other conditions.

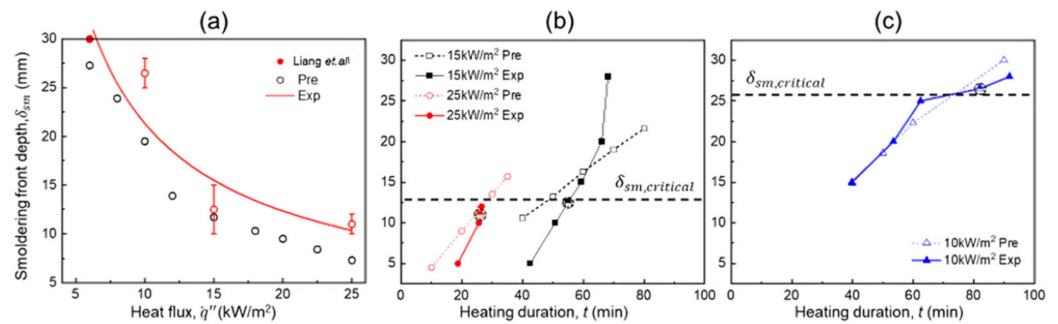


Figure 9. Predicted and experimental results (part from [40]) for critical (a) smoldering front depth, (b) heating duration for $T_c = 500$ °C at 15 and 25 kW/m², and (c) heating duration for $T_c = 350$ °C at 10 kW/m².

Notably, $\delta_{sm,min}$ calculated by Equation (4) only represents the critical condition of the material for restricted experimental conditions and the state that without external irradiation is unpredictable. Therefore, Equation (4) will be transformed as

$$\delta_{sm,min} = \frac{\dot{q}_{py}'' + \dot{q}_{loss}''}{\dot{q}_{sm}'''} \quad (5)$$

From the perspective of local energy balance, as illustrated in Figure 8b, the heat released from the char oxidation (\dot{q}_{sm}'') and the external irradiation (\dot{q}_{in}'') should be equal to the heat absorbed by pyrolysis (\dot{q}_{py}'') [15] and heat losses of the environment (\dot{q}_{loss}'') as

$$\dot{q}_{sm}'' + \dot{q}_{in}'' = \dot{q}_{py}'' + \dot{q}_{loss}'' \quad (6)$$

The net energy rate [36] (\dot{E}_{net}) of the smoldering front can be expressed as

$$\dot{E}_{net} = R \left(\int_0^{\delta_{sm}} \dot{q}_{ox}'' dx + \int_0^{\delta} \dot{q}_{in}'' dx - \int_0^{\delta - \delta_{sm}} \dot{q}_{py}'' dx - \int_0^{\delta} \dot{q}_{loss}'' dx \right) \quad (7)$$

and R is the diameter of the specimen. Considering the limited heating duration (t), the net energy (E_{net}) should equal the stored energy of the smoldering front:

$$E_{net} = \int_0^t \dot{E}_{net} dt = \rho R \delta \phi c_p T_c \delta_{sm} \quad (8)$$

Figure 9b,c show the predicted and experimental smoldering front depth (δ_{sm}) as a function of heating duration (t) for $T_c = 500$ °C at 15 and 25 kW/m² and $T_c = 350$ °C at 10 kW/m². The smoldering depth is linear with the heating duration for both characteristic temperatures. For a certain depth, the required heating duration is lower at a high heat flux. The dashed line represents the critical depth ($\delta_{sm,critical}$) for self-sustained smoldering without external irradiation calculated by Equation (5), which is 12.7 mm for $T_c = 500$ °C

and 25.7 mm for $T_c = 350$ °C. The related heating duration from the equation is 28 min at 25 kW/m², 58 min at 15 kW/m², and 74 min at 10 kW/m², basically consistent with the experimental results. The deviation may result from the multiple reactions and convective and radiative effects, which are difficult to quantify.

5. Conclusions

In this work, a series of experiments were performed to characterize the criterion of self-sustained and self-extinguished smoldering of beech (diameter of 60 mm, thickness of 30 mm). Features of self-extinguished and self-sustained smoldering are observed. For self-extinguished smoldering, temperatures will quickly drop below 300 °C, and the mass loss rate will gradually decrease to below 1 g/(m²·s) as well. For self-sustained smoldering, internal temperatures can still reach T_c , and this level can be maintained. The characteristic temperature and smoldering front depth are well defined. For a certain heat flux, as the smoldering front depth increases, the propagation speed and thermocouple measurement will become closer to the condition of the maximum smoldering front depth (30 mm), for which external radiation is always maintained. It can be speculated that external radiation will no longer have impacts on smoldering propagation once the smoldering is self-sustained.

The critical smoldering front depth of self-extinguished and self-sustained smoldering is 10–15 mm for 30 mm thick wood at 15.5 kW/m². This depth will decrease with the increase in heat flux, from 26.5 ± 1.5 mm at 10 kW/m² to 11 ± 1 mm at 25 kW/m². However, when the heat flux is increased from 15 to 25 kW/m², the critical depth changes slightly. For 30 mm thick wood, once the critical depth is reached, self-sustained smoldering easily occurs, and the influence of external heat flux will become small. Furthermore, the smoldering behavior of the specimen can be divided into self-sustained and self-extinguished smoldering regions for different heat fluxes and smoldering front depths.

Energy-conservation equations based on local energy balance are proposed to explain and predict the critical smoldering front depth of self-extinguished and self-sustained smoldering. The model predicts that critical depth will decrease with an increase in heat flux, from 23.9 mm at 8 kW/m² to 7.3 mm at 25 kW/m², and the predicted critical depth is slightly lower than that in the experiment. The minimum depth for self-sustained smoldering without external irradiation is 12.7 mm for $T_c = 500$ °C and 25.7 mm for $T_c = 350$ °C. The related heating duration from the equation is 28 min at 25 kW/m², 58 min at 15 kW/m², and 74 min at 10 kW/m², basically consistent with the experimental results. This study proposes a feasible parameter, helping understand the threshold of smoldering propagation and the development of biomass burners.

Author Contributions: Conceptualization, P.D.; methodology, P.D., C.Z. and Q.H.; formal analysis, P.D. and C.Z.; investigation, P.D. and C.Z.; resources, L.W., Q.H. and Y.Y.; data curation, P.D. and C.Z.; writing—original draft preparation, P.D.; writing—review and editing, Q.H. and Y.Y.; supervision, L.W., Q.H. and Y.Y.; project administration, Q.H. and Y.Y.; funding acquisition, P.D., Q.H. and Y.Y. All authors have read and agreed to the published version of the manuscript.

Funding: This work was sponsored by the Shanghai Sailing Program (22YF1452400), Fundamental Research Funds for the Central Public Welfare Research Institutes (22SX16), MEM Key Laboratory of Fire Fighting and Rescue Technology and Equipment Project (2022QX08), and Anhui Provincial Natural Science Foundation (2208085QE160).

Institutional Review Board Statement: Not applicable.

Informed Consent Statement: Not applicable.

Data Availability Statement: The data presented in this study are available on request from the corresponding author. The data are not publicly available due to privacy issues.

Conflicts of Interest: The authors declare no conflicts of interest.

Appendix A

Figure A1 illustrates an example of the repetition of the experiment. It shows the error for the temperature gradient of 15 mm smoldering depth under the irradiation of 15.5 kW/m^2 .

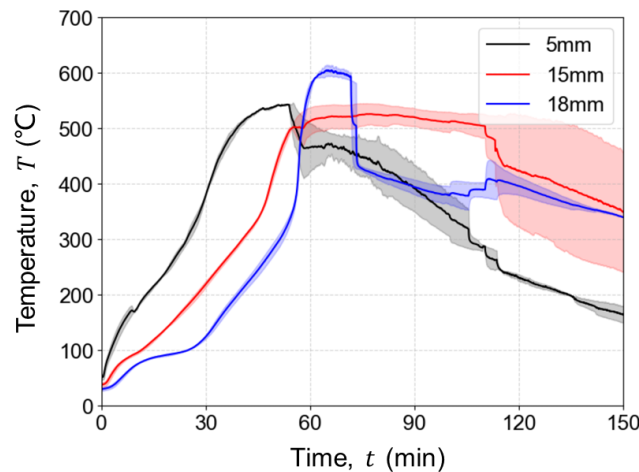


Figure A1. The error for the temperature gradient of 15 mm smoldering depth under the irradiation of 15.5 kW/m^2 .

References

- MacDicken, K.G. Global Forest Resources Assessment 2015: What, Why and How? *For. Ecol. Manag.* **2015**, *352*, 3–8. [[CrossRef](#)]
- Ramage, M.H.; Burrige, H.; Busse-Wicher, M.; Fereday, G.; Reynolds, T.; Shah, D.U.; Wu, G.; Yu, L.; Fleming, P.; Densley-Tingley, D.; et al. The Wood from the Trees: The Use of Timber in Construction. *Renew. Sustain. Energy Rev.* **2017**, *68*, 333–359. [[CrossRef](#)]
- Leslie, A.D.; Mencuccini, M.; Perks, M. The Potential for Eucalyptus as a Wood Fuel in the UK. *Appl. Energy* **2012**, *89*, 176–182. [[CrossRef](#)]
- Quintiere, J.G. *Fundamentals of Fire Phenomena*; Wiley: Hoboken, NJ, USA, 2006; ISBN 0470091134.
- Lin, S.; Huang, X.; Gao, J.; Ji, J. Extinction of Wood Fire: A Near-Limit Blue Flame above Hot Smoldering Surface. *Fire Technol.* **2022**, *58*, 415–434. [[CrossRef](#)]
- Wang, S.; Ding, P.; Lin, S.; Gong, J.; Huang, X. Smoldering and Flaming of Disc Wood Particles under External Radiation: Autoignition and Size Effect. *Front. Mech. Eng.* **2021**, *7*, 65. [[CrossRef](#)]
- Lin, S.; Huang, X.; Urban, J.; McAllister, S.; Fernandez-Pello, C. Piloted Ignition of Cylindrical Wildland Fuels under Irradiation. *Front. Mech. Eng.* **2019**, *5*, 54. [[CrossRef](#)]
- Wang, S.; Ding, P.; Lin, S.; Huang, X.; Usmani, A. Deformation of Wood Slice in Fire: Interactions between Heterogeneous Chemistry and Thermomechanical Stress. *Proc. Combust. Inst.* **2021**, *38*, 5081–5090. [[CrossRef](#)]
- Safdari, M.S.; Amini, E.; Weise, D.R.; Fletcher, T.H. Heating Rate and Temperature Effects on Pyrolysis Products from Live Wildland Fuels. *Fuel* **2019**, *242*, 295–304. [[CrossRef](#)]
- Chen, G.; Shiyuan, L.; Linwei, W. Current Investigation Status of Oxy-Fuel Circulating Fluidized Bed Combustion. *Fuel* **2023**, *342*, 127699. [[CrossRef](#)]
- Fawaz, M.; Lautenberger, C.; Bond, T.C. Prediction of Organic Aerosol Precursor Emission from the Pyrolysis of Thermally Thick Wood. *Fuel* **2020**, *269*, 117333. [[CrossRef](#)]
- Rein, G. Smoldering Combustion. In *SFPE Handbook of Fire Protection Engineering*; Springer: New York, NY, USA, 2014; pp. 581–603. [[CrossRef](#)]
- Rein, G. Smoldering Fires and Natural Fuels. In *Fire Phenomena and the Earth System*; John Wiley & Sons, Ltd.: Hoboken, NJ, USA, 2013; pp. 15–33. ISBN 9781118529539.
- Zanoni, M.A.B.; Torero, J.L.; Gerhard, J.I. Experimental and Numerical Investigation of Weak, Self-Sustained Conditions in Engineered Smoldering Combustion. *Combust. Flame* **2020**, *222*, 27–35. [[CrossRef](#)]
- Emberley, R.; Inghelbrecht, A.; Yu, Z.; Torero, J.L. Self-Extinction of Timber. *Proc. Combust. Inst.* **2017**, *36*, 3055–3062. [[CrossRef](#)]
- Emberley, R.; Putynska, C.G.; Bolanos, A.; Lucherini, A.; Solarte, A.; Soriguer, D.; Gonzalez, M.G.; Humphreys, K.; Hidalgo, J.P.; Maluk, C.; et al. Description of Small and Large-Scale Cross Laminated Timber Fire Tests. *Fire Saf. J.* **2017**, *91*, 327–335. [[CrossRef](#)]
- Emberley, R.; Do, T.; Yim, J.; Torero, J.L. Critical Heat Flux and Mass Loss Rate for Extinction of Flaming Combustion of Timber. *Fire Saf. J.* **2017**, *91*, 252–258. [[CrossRef](#)]
- Rein, G. Smoldering Combustion Phenomena in Science and Technology. *Int. Rev. Chem. Eng.* **2009**, *1*, 3–18.
- Ohlemiller, T.J. Modeling of Smoldering Combustion Propagation. *Prog. Energy Combust. Sci.* **1985**, *11*, 277–310. [[CrossRef](#)]

20. Lin, S.; Huang, X. Quenching of Smoldering: Effect of Wall Cooling on Extinction. *Proc. Combust. Inst.* **2021**, *38*, 5015–5022. [[CrossRef](#)]
21. Rashwan, T.L.; Torero, J.L.; Gerhard, J.I. Heat Losses in a Smoldering System: The Key Role of Non-Uniform Air Flux. *Combust. Flame* **2021**, *227*, 309–321. [[CrossRef](#)]
22. Kadowaki, O.; Suzuki, M.; Kuwana, K.; Nakamura, Y.; Kushida, G. Limit Conditions of Smoldering Spread in Counterflow Configuration: Extinction and Smoldering-to-Flaming Transition. *Proc. Combust. Inst.* **2021**, *38*, 5005–5013. [[CrossRef](#)]
23. Torero, J.L.; Gerhard, J.I.; Martins, M.F.; Zannoni, M.A.B.; Rashwan, T.L.; Brown, J.K. Processes Defining Smoldering Combustion: Integrated Review and Synthesis. *Prog. Energy Combust. Sci.* **2020**, *81*, 100869. [[CrossRef](#)]
24. Wang, S.; Huang, X.; Chen, H.; Liu, N. Interaction between Flaming and Smoldering in Hot-Particle Ignition of Forest Fuels and Effects of Moisture and Wind. *Int. J. Wildland Fire* **2017**, *26*, 71–81. [[CrossRef](#)]
25. Xie, Q.; Zhang, Z.; Lin, S.; Qu, Y.; Huang, X. Smoldering Fire of High-Density Cotton Bale Under Concurrent Wind. *Fire Technol.* **2020**, *56*, 2241–2256. [[CrossRef](#)]
26. Wang, Q.; Liu, K.; Wang, S. Effect of Porosity on Ignition and Burning Behavior of Cellulose Materials. *Fuel* **2022**, *322*. [[CrossRef](#)]
27. Ohlemiller, T.J. Smoldering Combustion Propagation on Solid Wood. In *Fire Safety Science: Proceedings of the Third International Symposium, Edinburgh, Scotland, 8–12 July 1991*; Routledge: London, UK, 1991; pp. 565–574. [[CrossRef](#)]
28. Torero, J.L.; Fernandez-Pello, A.C.; Kitano, M. Opposed Forced Flow Smoldering of Polyurethane Foam. *Combust. Sci. Technol.* **1993**, *91*, 95–117. [[CrossRef](#)]
29. Yamazaki, T.; Matsuoka, T.; Nakamura, Y. Near-Extinction Behavior of Smoldering Combustion under Highly Vacuumed Environment. *Proc. Combust. Inst.* **2019**, *37*, 4083–4090. [[CrossRef](#)]
30. Gratkowski, M.T.; Dembsey, N.A.; Beyler, C.L. Radiant Smoldering Ignition of Plywood. *Fire Saf. J.* **2006**, *41*, 427–443. [[CrossRef](#)]
31. Miry, S.Z.; Zannoni, M.A.B.; Rashwan, T.L.; Torero, J.L.; Gerhard, J.I. Investigation of Multi-Dimensional Transfer Effects in Applied Smoldering Systems: A 2D Numerical Modelling Approach. *Combust. Flame* **2022**, *246*, 112385. [[CrossRef](#)]
32. Rashwan, T.L.; Fournie, T.; Green, M.; Duchesne, A.L.; Brown, J.K.; Grant, G.P.; Torero, J.L.; Gerhard, J.I. Applied Smoldering for Co-Waste Management: Benefits and Trade-Offs. *Fuel Process. Technol.* **2023**, *240*, 107542. [[CrossRef](#)]
33. Linan, A. The Asymptotic Structure of Counterflow Diffusion Flames for Large Activation Energies. *Acta Astronaut.* **1974**, *1*, 1007–1039. [[CrossRef](#)]
34. Dosanjh, S.S.; Pagni, P.J.; Fernandez-Pello, A.C. Forced Cocurrent Smoldering Combustion. *Combust. Flame* **1987**, *68*, 131–142. [[CrossRef](#)]
35. Zannoni, M.A.B.; Torero, J.L.; Gerhard, J.I. Delineating and Explaining the Limits of Self-Sustained Smoldering Combustion. *Combust. Flame* **2019**, *201*, 78–92. [[CrossRef](#)]
36. Zannoni, M.A.B.; Torero, J.L.; Gerhard, J.I. Determining the Conditions That Lead to Self-Sustained Smoldering Combustion by Means of Numerical Modelling. *Proc. Combust. Inst.* **2019**, *37*, 4043–4051. [[CrossRef](#)]
37. Huang, X.; Rein, G. Downward Spread of Smoldering Peat Fire: The Role of Moisture, Density and Oxygen Supply. *Int. J. Wildland Fire* **2017**, *26*, 907–918. [[CrossRef](#)]
38. Huang, X.; Rein, G. Upward-and-Downward Spread of Smoldering Peat Fire. *Proc. Combust. Inst.* **2019**, *37*, 4025–4033. [[CrossRef](#)]
39. Wang, Z.; Liu, N.; Yuan, H.; Chen, H.; Xie, X.; Zhang, L.; Rein, G. Smoldering and Its Transition to Flaming Combustion of Polyurethane Foam: An Experimental Study. *Fuel* **2022**, *309*, 122249. [[CrossRef](#)]
40. Liang, Z.; Lin, S.; Huang, X. Smoldering Ignition and Emission Dynamics of Wood under Low Irradiation. *Fire Mater.* **2022**, *47*, 514–524. [[CrossRef](#)]

Disclaimer/Publisher’s Note: The statements, opinions and data contained in all publications are solely those of the individual author(s) and contributor(s) and not of MDPI and/or the editor(s). MDPI and/or the editor(s) disclaim responsibility for any injury to people or property resulting from any ideas, methods, instructions or products referred to in the content.